Detection and Monitoring of Brain Stroke Onsets by an Ad-hoc Double Stage Delay-Multiply-And-Sum (DS-DMAS) Algorithm

URSI-B EMTS 2025, Bologna, 23–27 June

Detection and Monitoring of Brain Stroke Onsets by an Ad-hoc Double Stage Delay-Multiply-And-Sum (DS-DMAS) Algorithm

Alex R. Masaquiza Caiza, David O. Rodriguez-Duarte, and Francesca Vipiana
Department of Electronics and Telecommunications, Politecnico di Torino, 10129 Torino, Italy

Abstract

This paper presents an ad hoc Double-Stage Multiply-Delay-and-Sum (DS-DMAS) confocal algorithm with a pre-calibration stage and simplified wave propagation compensation adapted for microwave-imaging-based detection and monitoring of brain stroke onsets. We numerically assesses the algorithm using mimicked clinical scenarios of detection and follow-up, including a setup with a multi-view 22-antennas system operating from 0.8 to 1.8 GHz and both anthropomorphic homogeneous and multi-tissue head models. The results demonstrate the capability to detect and monitor the pathology, providing 3D intensity power maps highlighting the evolving stroke-affected areas.

1 Introduction

Brain stroke is a relevant worldwide health concern, rating mortality in disability incidence of millions per year. It consists of either artery occlusions or vessel burns that provoke ischemia (IS) or intracranial hemorrhages (ICH), respectively, triggering brain cell death in the affected areas and generating dielectric contrast variations. For instance, IS causes a substantial decline in oxygen and nutrients, reflected in lower permittivity at the microwave range, and conversely, ICH causes a rise. These dielectric contrasts allow microwave imaging (MWI) systems to process and reconstruct dielectric maps that indicate the pathology's location and/or progression [1], acting like a support instrument of diagnosis. MWI technology provides a low-cost and harmless alternative to diagnosis and follow-up, complementing the current gold standards of Computed Tomography (CT) and Magnetic Resonant Imaging (MRI).

An MWI device comprises two main parts: a hardware one, usually consisting of an array of antennas and a transceiving module, and a software one, covering the imaging retrieval algorithms [2], classified in quantitative and qualitative. The quantitative, also known as tomographic, generates dielectric maps via inversion algorithms. The qualitative ones retrieve intensity maps instead, requiring less computational load, albeit with less information. However, qualitative information, such as location and shape estimation, is still valuable medical data that can guide interventions.

Confocal radar-based methods such as Delay-And-Sum (DAS), Delay-Multiply-And-Sum (DMAS), or Double-Stage DMAS (DS-DMAS) are widely used qualitative approaches for brain stroke detection. In [3], the authors use an optimized DAS that balances the speed of the propagation wave within a complex region to detect the stroke presence, while [4], [5] present enhanced confocal algorithms with join calibration procedures to image ICH cases.

This work proposes a DS-DMAS with a simplified wave propagation scheme and adaptable calibration stage that suits the realistic constraints of brain stroke detection and follow-up, like the variability of the patient morphology. To test it, we perform a numerical analysis of different stroke conditions using full-wave simulations done by an in-house EM finite element (FEM) solver and 3D homogeneous and multi-tissue anthropomorphic models of the head [6], while the reference MWI system presented in [7], comprising a 22-monopole antenna array with discrete matching medium modules operating in a narrowband from 0.8 to 1.8 GHz.

2 The Imaging Algorithm

DAS, also known as confocal MWI, is a well-known correlation-based method [8], [9] in which time-domain signals are synthetically focused at a specific point in the imaging domain (DoI). It images by migrating pulsed signals [10], and computing the spatial permittivity distributions by processing the back-scattered signals. It has been used for medical imaging purposes in cases of early-stage breast cancer and brain stroke detection [11]–[13]. Specifically, in this work, we employ a DS-DMAS computing the energy distribution coherently, which is enhanced with clutter suppression and baseline calibration.

2.1 Clutter Suppression

The collected time-domain back-scattered signals used for the imaging contain early- and late-time responses. The incident pulse and reflections from the immediate domains dominate the early-time content, e.g., antenna-matching medium and skin, and the stroke and internal tissues backscatter the late-time content. Thus, we apply adequate signal processing based on a time-gating approach to remove early-time content that generally has a greater ampli-

tude than the stroke one, suppressing the clutter response and enhancing the overall imaging.

2.2 Baseline Calibration

The baseline calibration is a two-fold procedure that reduces the remaining clutter effects and allows monitoring by differentiating baseline time signals, ζ_n^{ref}, from the target ones, ζ_n^{tgt}, i.e., the raw measured backscattered signals, where n-th indicates the antenna index. This difference results in the input of the later-used DS-DMAS, $d_n = \zeta_n^{\text{tgt}} - \zeta_n^{\text{ref}}$. Then, to obtain ζ^{ref}, a reference scenario is considered depending on the availability, which could be, for instance, one using a healthy head model, the tested head in a preliminary state—one before the examination—or even one averaging all head tissues in a single homogeneous one. Here, it is worth noticing the practical clinical implication of the assumption that would allow for both scenarios of detection and monitoring.

2.3 DS-DMAS Confocal Imaging

For the imaging process, we employ the DS-MDAS approach, as outlined in Algorithm 1, which iterates over each focal point $\vec{r} \in$ DoI. For each antenna n, the corresponding time delay is determined like $\tau_i(\vec{r}) = 2|\vec{r} - \vec{r}_i|/v$, where $|\vec{r} - \vec{r}_i|$ indicates the distance between the antenna location, $\vec{r}_i$, and the focal point, $\vec{r}$, and v is the velocity of signal propagation in the medium. Then, the contributions from the n-th antenna are time-shifted, aligning them to the focal point of interest. The obtained contributions, $B_i(t - \tau_i(\vec{r}))$, are summed coherently to be processed in two multiplication stages (lines 7 to 13 of Algorithm 1). At the end of these stages, the resulting signal, $D_i(t,\vec{r})$, is normalized (line 14 of Algorithm 1). Finally, all contributions are summed into a unique signal as

$$S(\vec{r}) = \sum_{i=1}^{n} E_i(t,\vec{r}), \tag{1}$$

and the intensity $I(\vec{r})$ for each focal point is computed by integrating this signal in the time domain as expressed as

$$I(\vec{r}) = \int S(\vec{r},t)\,dt, \tag{2}$$

that are assigned to the pixel at the focal point of interest. This process is repeated across all focal points, generating a 3D intensity map of the scattered energy.

Algorithm 1: DS-DMAS Beamforming Algorithm

Data: d_n from N antennas, DoI defined as a 3D grid of focal points $\vec{r}$, and propagation velocity of the signal $v(\vec{r})$

Result: 3D intensity map $I(\vec{r})$ of scattered energy.

1 **foreach** $\vec{r}$ **do**
2 Initialize $I(\vec{r}) = 0$;
3 **for** $n = 1$ *to* N **do**
4 Compute the time delay $\tau_i(\vec{r})$;
5 Extract the time-shifted signal $B_i(t - \tau_i(\vec{r}))$;
6 **end**
7 **for** $n = 1$ *to* N **do**
8 $j = (n \mod N) + 1$;
9 $C_i(t,\vec{r}) = B_i(t - \tau_i(\vec{r})) \cdot B_j(t - \tau_j(\vec{r}))$;
10 **end**
11 **for** $n = 1$ *to* N **do**
12 $j = (n \mod N) + 1$;
13 $D_i(t,\vec{r}) = C_i((\vec{r})) \cdot C_j((\vec{r}))$;
14 $E_i(t,\vec{r}) = sign(D_i(t,\vec{r})) \cdot \sqrt{|D_i(t,\vec{r})|}$;
15 **end**
16 Compute the coherent sum of contributions: $S(\vec{r})$;
17 Assign intensity value to focal point: $I(\vec{r})$;
18 **end**

3 Numerical Assessment

As mentioned in the introduction, to assess the proposed approach, we consider the 22-antenna MWI system placed around the head in two-ring arrays [7] and full-wave simulations using an EM in-house FEM solver and realistic head models [6], mimicking detection and monitoring scenarios. The frequency band considered for the simulation ranged from 0.8 to 1.8 GHz, using twenty-one samples evenly spaced by 50 MHz.

3.1 Stroke Detection

To test the detection and localization capabilities of the proposed approach, we mimic an ICH employing a spherical 10cm^3-radio target, homogeneously filled with a material with blood properties, that is localized at different positions within the brain area. Then, the first assessment, and the least complex of the studies cases, considers a single tissue head filled homogeneously with a material averaging the properties of the head. In this case, we use the head without a stroke as a calibration reference and three different ICHs as targets, as signaled by the red contour lines in Fig. 1. Moreover, the calculation of v assumes the same single-tissue non-stroke scenario.

Figure 1 shows the retrieved intensity maps for all three cases, displayed in the standard, transverse, sagittal, and frontal views. From this, it is clear that strokes are always detected and, most of the time, well-localized, with more difficulty determining the z-component in the case of the stroke placed most internally. This is probably due to the lack of information on this axis since no antennas are placed on top of the head in the studied configuration [7].

Maintaining the same stroke positions, the second test employs a multi-tissue head composed of skin, fat, bone, CSF, gray matter, white matter, and cerebellum. However, for baseline calibration and v calculation, the homogeneous single-tissue non-stroke head model is considered. It is a valuable practical assumption from the clinical applicability point of view. Figure 2 gathers the results, which presented similar performance.

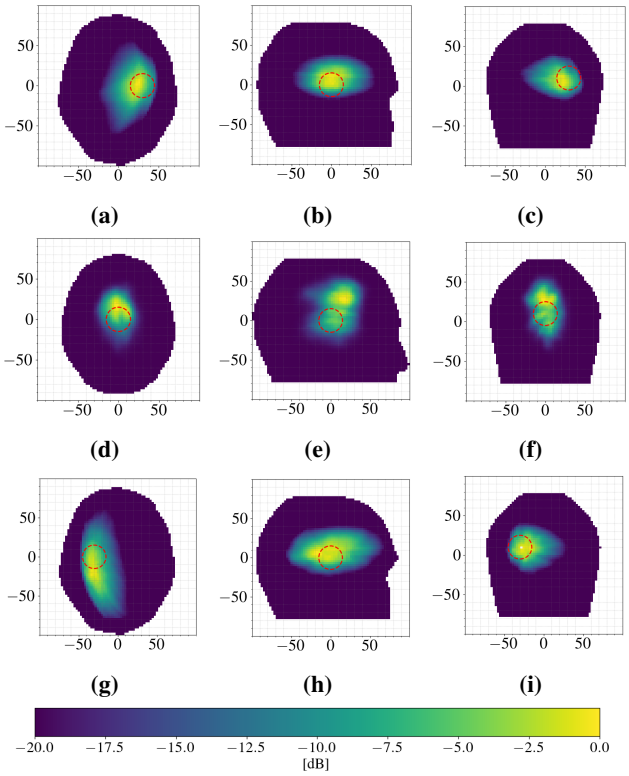

Figure 1. Normalized values of the reconstructed intensity map of a stroke at different locations using a single-tissue head model; (a-c) stroke located in the lateral left hemispherical region, (d-e) stroke located in the medial region, (g-i) stroke located in the lateral right hemispherical region

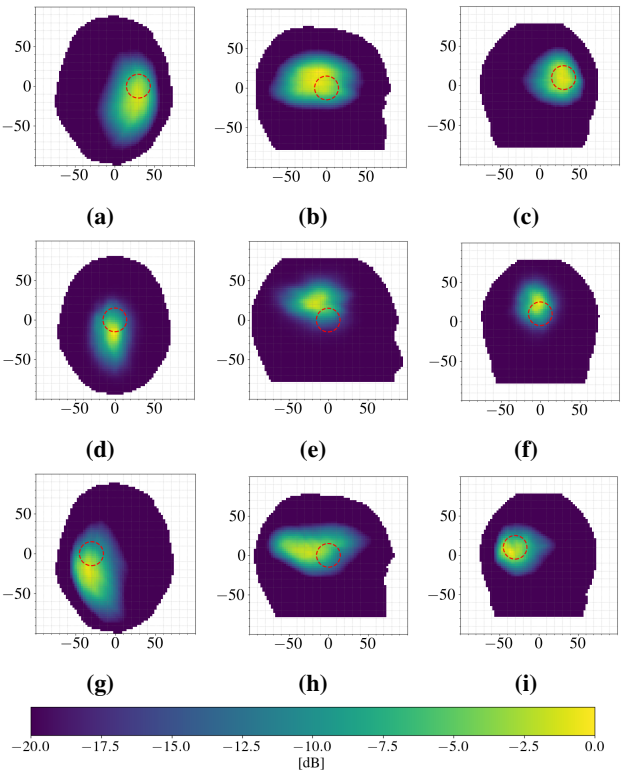

Figure 2. Normalized values of the reconstructed intensity map of strokes at different locations using a multi-tissue head model; (a-c) stroke located in the lateral left hemispherical region, (d-e) stroke located in the medial region, (g-i) stroke located in the lateral right hemispherical region

3.2 Stroke Monitoring

The detection and localization of brain strokes are crucial for the first evaluation. However, the follow-up is a fundamental unmet medical requirement with the potential to support the afterward interventions. In this section, we studied the feasibility of our approach to monitoring an evolving brain stroke onset. To that end, we employ the homogeneous head model while placing an ICH capsule-shaped stroke. Then, two changing states are considered: first, a healthy condition, at t_0, evolving to a 5-cm^3 stroke onset, at t_1, and second, from t_1, an axial growth reaching the 25-cm^3 at t_2. To monitor the changes in the stroke from one time instant t_{m-1} to another instant t_m over time, we used a calibrated signal d^{m-1} taken at time instant t_{m-1} as a reference signal for the subsequent monitoring stages. Hence, the differential signal contains information about the changes in the stroke volume. Moreover, we employ the homogeneous head model for the v computation, similar to the detection test.

Figure 3 shows the two monitoring studied cases, indicating in each case the variation zone. The results confirm the capability of the approach to perform the monitoring job, though limitations in the shape retrieval.

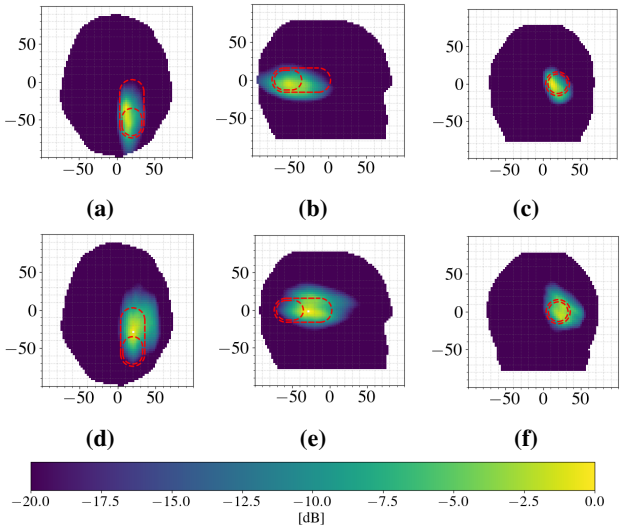

Figure 3. Monitoring of stroke onsets progression indicate whit normalized intensity maps; (a-c) Case 1: healthy condition to 5 cm^3 stroke, (d-f) Case 2: 5 to 25 cm^3 stroke.

3.3 Conclusions and Perspectives

The presented work validated the feasibility of the Double Stage Delay-Multiply-And-Sum (DS-DMAS) algorithm together with clutter suppression and a baseline calibration for the detection and monitoring of brain onsets in realistic

clinical scenarios. The study outcomes demonstrated the system's reliability in detecting and localizing brain strokes of different volumes: 5, 25, and 45 cm^3 at different intracranial positions. Moreover, the MWI algorithm allows the follow-up of brain strokes, which is a promising application in clinical settings and hospitals. The confocal imaging algorithm exposed in this work shows to be a reliable solution for brain stroke monitoring, requiring only a reference signal at any instant to follow up the evolution of a potential stroke effectively.

For the future, an experimental validation is planned, as well as further improvement and tuning of the algorithm.

4 Acknowledgements

This work is carried out partially within the Agritech National Research Center, funded by the European Union Next-Generation EU (Piano Nazionale di Ripresa e Resilienza (PNRR) – MISSIONE 4 COMPONENTE 2, INVESTIMENTO 1.4 – D.D. 1032 17/06/2022, CN00000022), the research project "3BAtwin - Bone, Brain, Breast and Axillary Medical Microwave Imaging Twinning" funded by Horizon Europe Framework Programme (101159623), and the research project "MedWaveImage - Microwave imaging technology transfer to innovate the medical sector", funded by Interreg Central Europe (CE0200670).

References

[1] C. Origlia, D. O. Rodriguez-Duarte, J. A. Tobon Vasquez, J.-C. Bolomey, and F. Vipiana, "Review of microwave near-field sensing and imaging devices in medical applications," *Sensors*, vol. 24, no. 14, 2024. DOI: 10.3390/s24144515.

[2] L. Guo, A. S. M. Alqadami, and A. Abbosh, "Stroke diagnosis using microwave techniques: Review of systems and algorithms," *IEEE Journal of Electromagnetics, RF and Microwaves in Medicine and Biology*, vol. 7, no. 2, pp. 122–135, 2023. DOI: 10.1109/JERM.2022.3227724.

[3] L. Guo and A. M. Abbosh, "Optimization-based confocal microwave imaging in medical applications," *IEEE Transactions on Antennas and Propagation*, vol. 63, no. 8, pp. 3531–3539, 2015. DOI: 10.1109/TAP.2015.2434394.

[4] B. Sohani, B. Khalesi, N. Ghavami, *et al.*, "Detection of haemorrhagic stroke in simulation and realistic 3-d human head phantom using microwave imaging," *Biomedical Signal Processing and Control*, vol. 61, p. 102 001, 2020. DOI: https://doi.org/10.1016/j.bspc.2020.102001.

[5] A. Trakic, A. Brankovic, A. Zamani, *et al.*, "Expedited stroke imaging with electromagnetic polar sensitivity encoding," *IEEE Transactions on Antennas and Propagation*, vol. 68, no. 12, pp. 8072–8081, 2020. DOI: 10.1109/TAP.2020.2996810.

[6] D. O. Rodriguez-Duarte, J. A. T. Vasquez, R. Scapaticci, L. Crocco, and F. Vipiana, "Assessing a microwave imaging system for brain stroke monitoring via high fidelity numerical modelling," *IEEE Journal of Electromagnetics, RF and Microwaves in Medicine and Biology*, vol. 5, no. 3, pp. 238–245, 2021.

[7] D. O. Rodriguez-Duarte, C. Origlia, J. A. T. Vasquez, R. Scapaticci, L. Crocco, and F. Vipiana, "Experimental assessment of real-time brain stroke monitoring via a microwave imaging scanner," *IEEE Open Journal of Antennas and Propagation*, vol. 3, pp. 824–835, 2022. DOI: 10.1109/OJAP.2022.3192884.

[8] H. Xia, Y. Ma, K. Yang, R. Cao, P. Chen, and H. Li, "Delay-and-sum beamforming based on the diagonal reducing method," in *OCEANS 2017 - Aberdeen*, 2017, pp. 1–5. DOI: 10.1109/OCEANSE.2017.8084592.

[9] M. Mozaffarzadeh, A. Mahloojifar, M. Orooji, S. Adabi, and M. Nasiriavanaki, "Double-stage delay multiply and sum beamforming algorithm: Application to linear-array photoacoustic imaging," *IEEE Transactions on Biomedical Engineering*, vol. 65, no. 1, pp. 31–42, 2018. DOI: 10.1109/TBME.2017.2690959.

[10] N. K. Nikolova, *Introduction to microwave imaging*. Cambridge University Press, 2017.

[11] G. Matrone, A. S. Savoia, G. Caliano, and G. Magenes, "The delay multiply and sum beamforming algorithm in ultrasound b-mode medical imaging," *IEEE Transactions on Medical Imaging*, vol. 34, no. 4, pp. 940–949, 2015. DOI: 10.1109/TMI.2014.2371235.

[12] H. Been Lim, N. Thi Tuyet Nhung, E.-P. Li, and N. Duc Thang, "Confocal microwave imaging for breast cancer detection: Delay-multiply-and-sum image reconstruction algorithm," *IEEE Transactions on Biomedical Engineering*, vol. 55, no. 6, pp. 1697–1704, 2008. DOI: 10.1109/TBME.2008.919716.

[13] S. Mustafa, B. Mohammed, and A. Abbosh, "Novel preprocessing techniques for accurate microwave imaging of human brain," *IEEE Antennas and Wireless Propagation Letters*, vol. 12, pp. 460–463, 2013. DOI: 10.1109/LAWP.2013.2255095.